Frequency Offset Tolerant Demodulation for Low Data Rate and Narrowband Wireless Sensor Node

Siavash Safapourhajari, André B. J. Kokkeler
University of Twente
Enschede, Netherlands
Email: s.safapourhajari@utwente.nl

***Abstract*— The issue of frequency offset in low data rate, narrowband and low power communication nodes is considered in this paper. To avoid power hungry precise frequency generation, offset tolerant demodulation and detection schemes are investigated. A Short-Time DFT (ST-DFT) based detection for BFSK is introduced which improves the BER performance of an existing design by almost 1dB. Its BER performance and complexity are also compared to frequency offset tolerant DDBPSK demodulation. Additionally, the effect of wider filter required to capture signal in presence of frequency offset is considered. The trade-off between performance and complexity for different offset values and filter bandwidths is discussed. Both methods work independent of frequency offset; however, it is shown that wider filters do not affect ST-DFT BER performance in contrast with DDBPSK. This robustness is obtained at the expense of increased computational load.**

Keywords—Discrete Fourier transforms, double differential modulation, frequency shift keying, phase shift keying, wireless sensor networks.

I. INTRODUCTION

The wide range of applications of wireless sensor networks has made them an attractive topic for research. These networks consisting of numerous small sensor nodes deployed densely in the area of interest, might be utilized for monitoring purposes in health care, security, environmental and home automation applications [1]. Given that most WSN applications require low data rates, an ultra-narrowband (UNB) communication scheme is emerging as a new approach to low data rate applications [2].

One of the well-known challenges in wireless communication systems is frequency offset cancellation. Frequency offset resulting from mismatch between local oscillators in the transmitter and receiver may considerably degrade system performance. Frequency offset can be handled and compensated in the analog domain, digital domain or both. Local oscillators usually work as a part of a Phase Locked Loop (PLL) so that frequency mismatch can be overcome by locking as close as possible to the nominal carrier frequency. Generally speaking, frequency is coarsely tuned in the analog domain (using a PLL) and the residual frequency offset is estimated and compensated after sampling the signal in the digital domain. A variety of algorithms has been proposed [3]–[7] to estimate and compensate for frequency offset in the digital domain for different modulation schemes. However, most of these methods are capable of handling frequency offsets up to a fraction of the data rate. Assume that the target data rate is 1kbps in the 2.4GHz band. For a frequency offset in the order of 20% of data rate, a frequency synthesizer with less than 0.2 part per million (ppm) deviation from nominal frequency is required. Even in case of 10kbps the required precision needs to be less than 2ppm which is too costly and power hungry to be affordable for a low power sensor node. Besides, the influence of frequency drift in such scenarios can be immensely destructive. In light of these facts one may think of exploiting demodulation and detection schemes which are able to tolerate frequency offset. It will relax the requirements of the crystal precision (and its thermal compensation) and PLL which leads to less power consumption [8].

Offset tolerant demodulation and detection schemes have been proposed to deal with large Doppler shift in space applications [9]–[12]. The Auto-Correlation Demodulator (ACD) is a well-known offset tolerant demodulation method for Double Differential BPSK (DDBPSK) [9], [10]. Another method which provides demodulation and detection independent of frequency offset for differentially encoded BFSK modulation is introduced in [11]. It is based on the Short-Time DFT (ST-DFT) of the received signal and aims at LEO satellite communication which must deal with large constant and largely variable frequency offsets. In [12] a DFT-based detector for a BFSK system is proposed which is robust against frequency offset. The authors have utilized 1-bit quantization and subsampling to achieve lower power consumption. They have also included a frequency tracking loop in their system to handle variable frequency offset.

To select an appropriate modulation technique for a wireless sensor node its BER performance and complexity must be taken into account for the intended application. In this paper, offset tolerant detection for BFSK and DDBPSK are compared to clarify the trade-off between BER performance, complexity and tolerable frequency offset. As for DDBPSK a conventional implementation is considered as in [9]. For offset tolerant BFSK detection an ST-DFT based detector is introduced to handle frequency offset and drift in low data rate wireless sensor nodes. It is a variation of [11] where a detection algorithm similar to [12] is employed. It uses a simpler detection algorithm compared

978-1-5386-2887-4/17/$31.00 ©2017 IEEE

to [11] while it achieves better performance by removing some performance degradation sources in [11].

The rest of this paper is organized as follows. ST-DFT detection for BFSK and ACD detection for DDBPSK are explained in sections II and III, respectively. Section IV contains simulation results and is followed by a discussion and comparison between the methods in section V. Finally, section VI concludes the paper.

II. Short-Time DFT (ST-DFT) detection for BFSK

Short-Time DFT is a time-frequency analysis which is obtained via calculating the DFT of a windowed portion of a signal. It demonstrates how frequency components of a signal change during time [13]. The information of frequency components obtained using such a time-frequency analysis method can be used for detecting FSK modulated data. The block diagram of an FSK ST-DFT based demodulator is depicted in Fig. 1.

As shown by Fig. 1, received samples go through an ST-DFT analysis block which is receiving timing information from a window synchronization block. Then the decision algorithm provides a data sequence based on the result of the ST-DFT analysis. In the following subsections the ST-DFT analysis, the detection algorithm and the window timing synchronization blocks are explicated.

A. Signal model and ST-DFT Analysis

The baseband signal model of BFSK in the n^{th} symbol interval is :

$$s(t) = \mathcal{R}e\{exp(j2\pi a_n(f_{sep}/2)t)\} \quad (1)$$

where a_n is the bipolar data (1 and -1) and f_{sep} is the frequency separation. The signal model in (1) is based on the assumption of using rectangular pulses and zero frequency and phase offset. If a pulse shape of $g(t)$ is used to suppress side lobes of the spectrum, continuous phase FSK is obtained and its baseband model during n^{th} symbol ($(n-1)T < t < nT$) is:

$$s(t) = exp\left(j \times \left\{\pi f_{sep} \sum_{k=1}^{n} a_k \int_0^t g(t-kT)dt\right\}\right) \quad (2)$$

where a_k is the bipolar data and T is the symbol period and $g(t)$ is the pulse shape. In BFSK, the bit period and symbol period are the same and in this paper they are referred to as symbol period, T.

Input samples pass through a window before frequency domain analysis is applied to them. Subsequently, zeros are added to the tail of the windowed samples. Given that the length of the window is L, $(I-1)$ times L zeros are added so that the overall length of sample sequence for each symbol becomes LI. The final input to the DFT block for the n^{th} symbol is:

$$s_{z,w}(n,m) = \begin{cases} s((n-1)T + mT_s)w(mT_s) & 1 \le m \le M \\ 0 & M < m \le M \times I \end{cases} \quad (4)$$

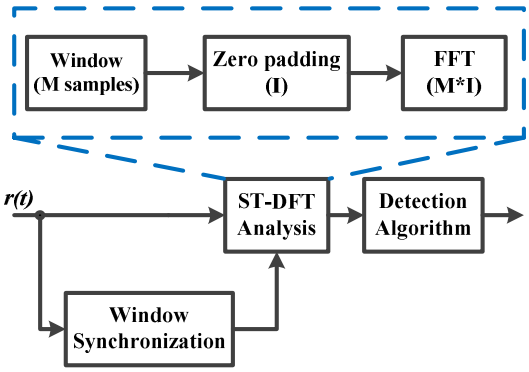

Fig. 1. Block diagram of ST-DFT based demodulator, where I is zero padding factor and M is the number of samples per symbol [11]

where M is the number of samples per symbol and the window length is considered to be equal to one symbol (L=M); m is an integer number showing the sample index, T_s is the sampling time, and I is the zero padding factor. In (4), $w(t)$ is the window function which is considered to be a rectangular function in this work.

At the output of the ST-DFT block, a time-frequency representation of the signal is obtained (5).

$$S_{STDFT}(n) = \{S_{n,k}\} \quad k = 0,1,2,\dots,MI-1 \quad (5\text{-}1)$$

$$S_{n,k} = \sum_{m=0}^{MI-1} s_{z,w}(n,m)exp(-j\frac{2\pi mk}{MI}) \quad (5\text{-}2)$$

The magnitude of $S_{n,k}$ determines the contribution of the k^{th} ST-DFT bin and its corresponding frequency to the signal during the n^{th} symbol interval.

In case of noise free operation the maximum value of the ST-DFT can be used to decide about the frequency of the transmitted signal; however, in a low SNR scenario, the ST-DFT bin, corresponding to the transmitted frequency does not necessarily have the maximum value (w. r. t. the other bins) due to noise. It particularly is more severe in our system as the DFT is calculated over a small set of signal samples in one symbol. Hence, a detection algorithm other than just maximum search is required to extract correct data.

B. Detection algorithm

Once samples pass through the ST-DFT analysis block, data can be detected based on the obtained time-frequency representation using a detection algorithm. In [11] for each symbol the output of the ST-DFT block is searched to find all peaks and the algorithm below is used for the detection of bits. The j^{th} bin of the spectrum is a peak if $S_{n,j} > S_{n,j-1}$ and $S_{n,j} > S_{n,j+1}$. Among all peaks, only one is the relevant peak corresponding to the frequency of the received signal and the others are the effect of noise. For each spectral peak the corresponding frequency is compared to the detected frequency in the previous symbol and a decision is made accordingly (6) [11].

$$f_d(j) = \left| f_{peak}^{j}(n) - f_{dec}(n-1) \right| \quad (6\text{-}1)$$

$$\begin{cases} f_d(j) \le f_{RES} & \hat{a}_n = 1, f_{dec}(n) = f_{peak}^{j}(n) \\ \left| f_d(j) - f_{sep} \right| \le f_{RES} & \hat{a}_n = -1, f_{dec}(n) = f_{peak}^{j}(n) \\ otherwise & go\ to\ peak\ (j+1) \end{cases} \quad (6\text{-}2)$$

where n is symbol index, j is the index of the current peak being investigated; f_{sep} denotes the separation between two frequencies in BFSK modulation; $f_{dec}(n-1)$ is the frequency decided for symbol *n-1* and f_{RES} is the frequency resolution of the ST-DFT which is the difference between frequencies of two adjacent bins within the ST-DFT analysis.

Utilizing this algorithm for a differentially encoded BFSK, constant frequency offset and variable frequency offset (the latter to some extent) will not affect Bit Error Rate (BER). To improve performance, in this paper two reasons that cause performance loss in [11] are eliminated. These include differential detection, which imposes a limit on system performance, and relying on peak detection for decision making. To understand why the latter may decrease the performance one needs to consider the effect of zero padding (which is equivalent to spectral interpolation). If a noisy signal *x(t)+n(t)* is zero padded with a factor of *I*, its DFT will be [14]:

$$\begin{aligned} X_I(\omega_l) &= \sum_{k=0}^{M-1} (X(\omega_k) + n_k) \left[\frac{1}{M} \sum_{m=0}^{M-1} exp(j(\omega_k - \omega_l)m) \right] \\ &= \left(\sum_{k=0}^{M-1} X(\omega_k) \left[\frac{1}{M} \sum_{m=0}^{M-1} exp(j(\omega_k - \omega_l)m) \right] \right) + n_I(l) \end{aligned} \quad (7)$$

where $X_I(\omega_l)$ is the interpolated spectrum of *x*, *l* is the interpolated spectrum frequency index and *l=0,1,..,MI-1*(*I* is zero padding factor and *M* is the number of samples), $X(\omega_k)$ (*k=0,1,...,M-1*) is the DFT of *x* without zero padding, n_k is the effect of noise on spectrum and $n_I(l)$ is the effect of noise on the interpolated spectrum.

As evidently seen, the noise effect in (7) can slightly change the value of a bin in the ST-DFT when spectral interpolation is utilized. Consequently, the frequency bin corresponding to a peak of the transmitted signal spectrum may deviate due to noise. This causes the peak frequency bin to be located outside the ranges defined in (6) for decision making and be dismissed as noise peak. Increasing the range may include these deviated frequency peaks but may also include noisy peaks which are not related to the transmitted frequency.

To obtain better BER performance, and decrease detection complexity, a detection algorithm similar to [12] is used. In order to detect data in the proposed scheme, ST-DFT bins corresponding to high and low frequencies of the employed BFSK modulation are needed. In contrast with [12] which uses a separate preamble for frequency acquisition and timing synchronization, in our system a single preamble is used for both purposes. The frequency bins corresponding to high and low frequency bins are calculated once in a packet during the window timing synchronization phase without any additional complexity compared to [11]. Once the high and low bins (b_H and b_L, respectively) are selected, the detection algorithm for each symbol is very simple. The decision is made by comparing values of two ST-DFT bins (8).

$$\hat{a}_n = \begin{cases} 1 & S_{n,b_H} \ge S_{n,b_L} \\ -1 & otherwise \end{cases} \quad (8)$$

Fig. 2 depicts the modified ST-DFT based demodulator. The only drawback of our method is that all decisions are based on the ST-DFT bins selected at the beginning of the packet. That is to say, contrary to [11] our detection algorithm performance in presence of frequency drift is a function of packet size. A frequency drift results in a gradual deviation from originally selected bins. A slight deviation from main frequencies can be tolerated in our detection method; whereas, a serious problem rises if the packet size is so large that the frequency deviation is significant. Besides, in case of very long packets the probability of error increases when we get closer to the end of packet. However, the packet size in the target low data rate applications is small enough to prevent above mentioned problems [2].

C. *Window timing synchronization*

The window timing scheme used in this work is the same as in [11]. A preamble of alternating zeros and ones is sent at the beginning of each packet. Windows with different delays are considered. Two different peaks might be found in the ST-DFT result of different windows (for each window it is the result of accumulating all preamble symbols) and how the value of these two peaks change relative to each other determines where the window is located. If the window fits one symbol correctly the difference between the power in the two frequency bins corresponding to different transmitted frequencies is maximum (Fig. 3). Based on this observation from the preamble sequence, the window is synchronized with the incoming samples and two bins with maximum values are set as high and low frequency bins. Detailed analysis of the window timing synchronization algorithm can be found in [11]. BER performance curves of the ST-DFT method are presented in Section IV.

III. DOUBLE DIFFERENTIAL BPSK (DDBPSK)

Double differential detection has been proposed to detect BPSK in presence of frequency offset. One of the main architectures is the Auto-Correlation Demodulator (ACD) based

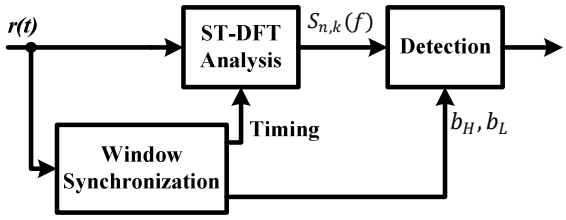

Fig. 2. Block diagram of the proposed ST-DFT demodulator

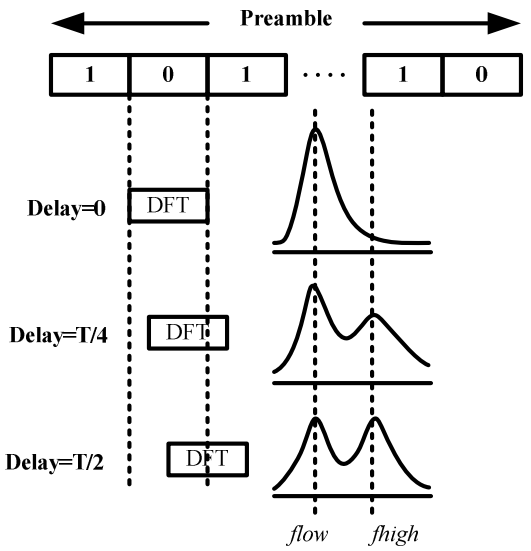

Fig. 3. Variation in spectrum when the window is delayed

detection [9]. The block diagram of an Auto-Correlation Demodulator for DPSK is shown in Fig. 4 where *r(t)* is complex envelope of signal and *(.)** denotes complex conjugate. In an optimum DPSK receiver the received samples are first integrated over bit intervals and then differential decoding is done using the result of these integrating blocks. In contrast, in ACDs, first the input data is multiplied by its delayed version and afterwards integrated over a symbol period.

A double differential detector utilizes a similar concept with an additional differential encoding in the transmitter and an additional decoder stage in the receiver. The block diagram of this double differential demodulator is demonstrated in Fig. 5. The error probability equation for such a system is derived and shown to be independent of frequency offset [9]. As an intuitive understanding it can be said that the first stage in Fig. 5 (delay and integration) converts the frequency offset to a constant phase term equivalent to $\Delta\omega T$ (where T is the symbol period and $\Delta\omega$ is frequency offset in radians per second); then, the rest of the diagram is a differential detector which can handle phase offset. As an enhancement, the second delay in the encoder and first

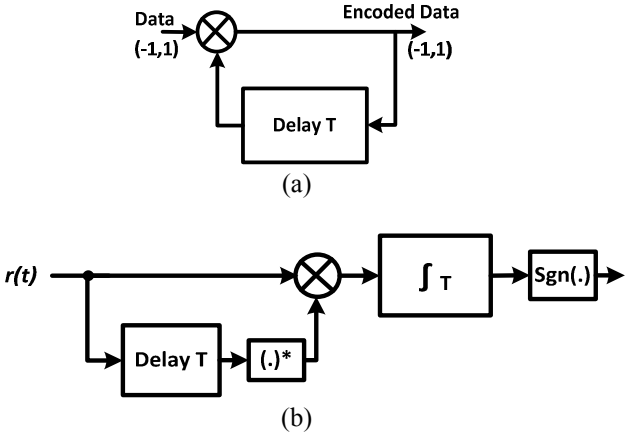

Fig. 4. Differential encoder (a) and ACD based demodulator for DPSK(b)

delay in the demodulator can be replaced by $2T$. It improves the performance as it decreases the noise sample correlations [9]. In this paper we consider the enhanced version of DDBPSK demodulator referred to as 2T-DDBPSK.

In the next section simulation results of ST-DFT and 2T-DDBPSK are presented. Complexity and performance trade-offs are discussed based on our simulation results.

IV. Simulation Results

Before presenting simulation results a brief clarification is needed regarding filtering in the system. Fig. 6 shows a simplified block diagram of the receiver. First, received RF signal passes through a bandpass filter (BPF). After amplification and down mixing in RF blocks an anti-aliasing filter (AA) filters the signal just before analog to digital converter. Further filtering and down-conversion might be also done in the digital domain before samples are sent to demodulator and detector. As illustrated in this block diagram different levels of filtering are performed before samples of data are processed. The higher tolerable frequency offset forces the bandwidth of these filters to increase (it also includes the RF filter in the front end). Here, filter bandwidth (F) refers to the single side bandwidth of the effective filter seen at the input of

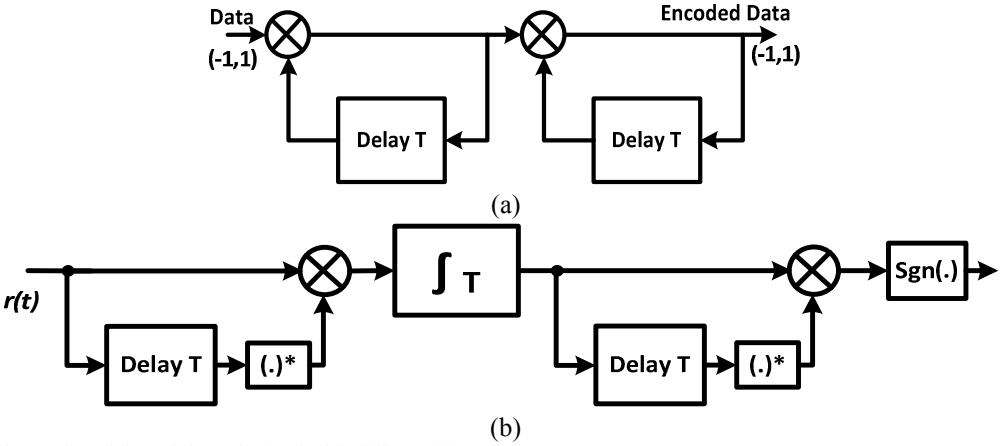

Fig. 5. Encoder (a) and ACD based demodulator (b) for double differential BPSK

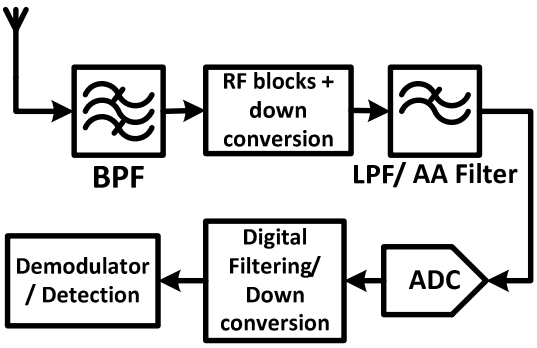

Fig. 6. Block diagram of receiver

the demodulator block. The effect of filtering emphasized in this paper is additional noise which is added to the signal compared to a conventional design without frequency offset. When there is no frequency offset, filters are tailored to a part of the spectrum which includes the signal and removes noise outside the signal band while this is not the case when wider filters are utilized in presence of frequency offset.

Extra noise due to a wider filter bandwidth is a crucial fact which cannot be ignored in offset tolerant demodulation methods. The filter bandwidth also determines how much frequency offset can be tolerated. The simulation results will be presented for normalized values of filter bandwidth (*FT* where *T* is symbol period) which is the same notation used in [9] . It provides tolerable offset values in terms of data rate. The relation between tolerable frequency offset, filter bandwidth and signal bandwidth is illustrated in Fig. 7 and equals:

$$\left|f_{offset,MAX}\right| = F - B_s/2 \qquad (9)$$

where B_s is the signal bandwidth. According to Carson's rule the approximate null to null bandwidth (B_s) of BFSK is $f_{sep} + 2R_b$, where R_b is data rate. As a result the approximated absolute value of maximum tolerable frequency offset (normalized) for ST-DFT based detection of BFSK when $f_{sep} = R_b$ is *FT-1.5*. Given that the BPSK signal bandwidth is roughly $2R_b$, the absolute value of maximum tolerable offset for DDBPSK would be *FT-1*.

For the ST-DFT simulations, a rectangular window of one symbol is exploited. The length of timing synchronization preamble is set to be 16 bits. The zero padding factor is 8 and packet size is assumed to be 1024 symbols both the same as [11].

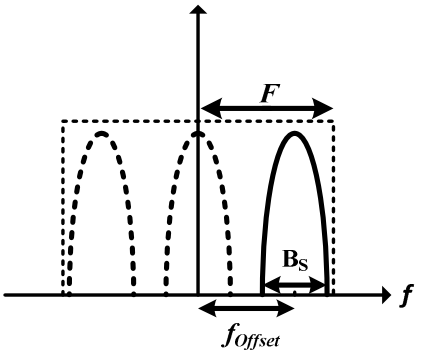

Fig. 7. Spectrum of filter and signal in presence of frequency offset

Frequency separation (f_{sep}) is equal to the data rate (R_b) which is the same as in [11]. The sampling frequency is considered such that it fulfills Nyquist criteria, namely, equal to the filter bandwidth (*F*) for complex samples.

Fig. 8 illustrates the BER curves for the introduced ST-DFT based BFSK detector when the pulse shape before frequency modulation is rectangular. Three different filter bandwidths are used including FT=8,16 and 32. It can be seen that the BER curves almost match those of non-coherent BFSK detection. The main difference is for E_b/N_0 less than 6dB where the window synchronization error degrades the performance of the method compared to non-coherent BFSK.

In order to make sure that our results can be fairly compared to [11], *g(t)* in (2) is chosen to be equal to the impulse response of a Raised Cosine filter. The roll-off factor of the raised cosine filter (α) is 1 which is the same as what used in [11].

Fig. 9 illustrates the BER curves for the proposed method with Raised Cosine pulse for three different values of *F*. BER curves for coherent and non-coherent BFSK are also demonstrated. Moreover, the error probability of [11] is presented which is almost 1 dB worse than our proposed method. Fig. 8 and Fig. 9 show that the performance is independent of the filter bandwidth if the filter is large enough to include the signal completely.

Fig. 10 demonstrates BER values for different E_b/N_0 values and different frequency drifts. As tolerable drift is affected by data rate, it is normalized to data rate so its dimension is *Hz/Symbol*. It can be seen that for a packet size of 1024 our method is able to tolerate considerably large values of frequency drift.

As mentioned in the previous section, if frequency drift and packet size are large the probability of erroneous detection at the beginning and end of the packet might be different. To investigate this difference, BER values for the first quarter and last quarter of a packet are calculated and shown in Fig. 11. The packet length is considered to be 1024 symbols and the number of iterations for BER calculation is set to be 10^4. The results demonstrate that when the drift is higher than 10% of data rate

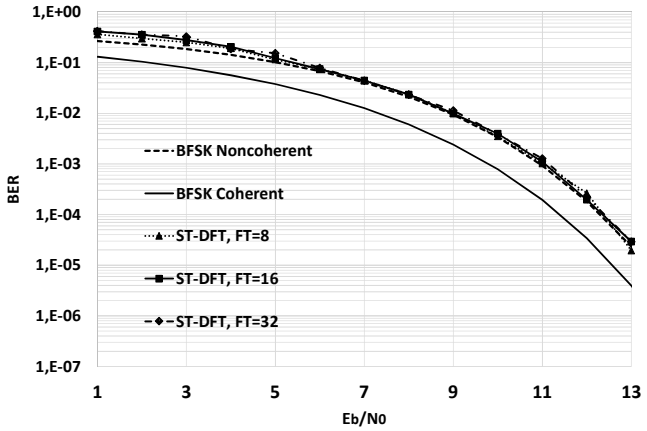

Fig. 8. BER curve for ST-DFT demodulation (Rectangular pulse shape) for three different filter bandwidths

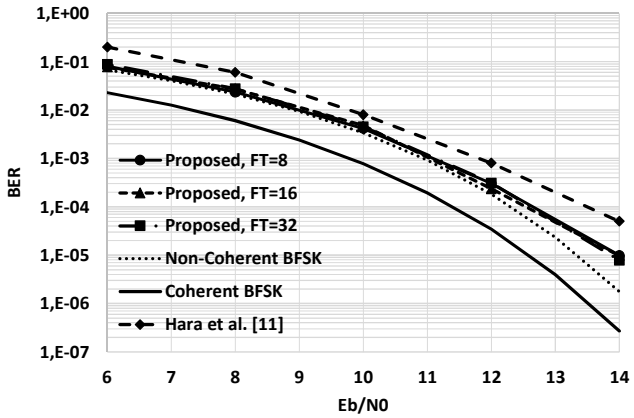

Fig. 9. BER curve for ST-DFT demodulation (Raised Cosine pulse shape) for three different filter bandwidths

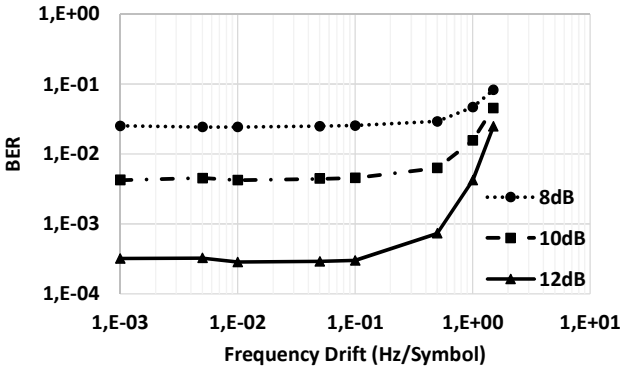

Fig. 10. BER of ST-DFT for E_b/N_0 of 8, 10 and 12 dB versus frequency drift

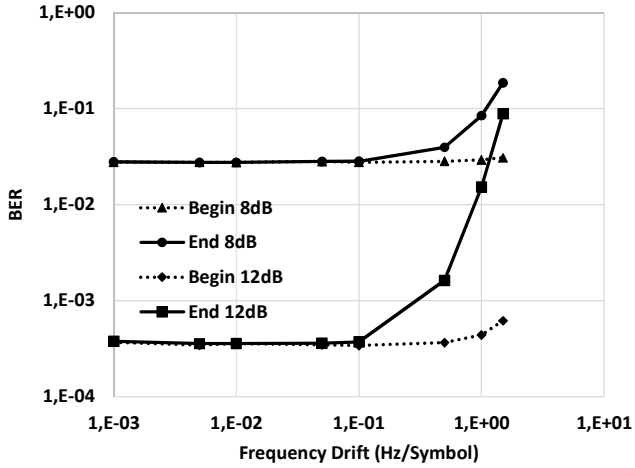

Fig. 11. BER at the first (Begin) and the last (End) quarter of a packet for different frequency drift values and two different E_b/N_0 values

the difference begins to increase and thus the detection is not reliable.

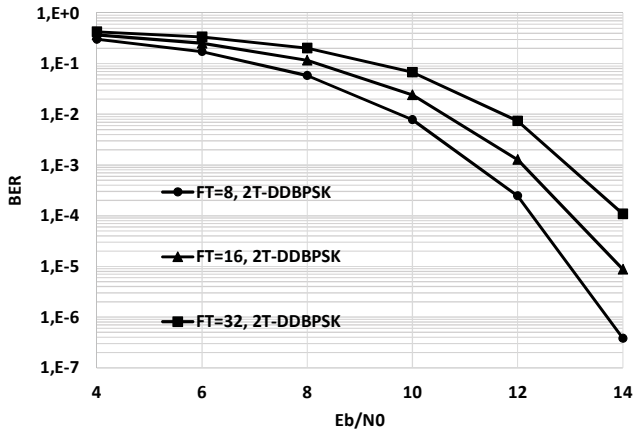

Fig. 12. BER curve for 2T-DDBPSK demodulation for three different filter bandwidths

The Bit Error Rate (BER) curves for 2T-DDBPSK are demonstrated in Fig. 12. The results are demonstrated for three different FT values; 8, 16 and 32.

V. Discussion and Comparison

A. *Effect of filter bandwidth*

A detection method might be able to tolerate frequency offset; nevertheless, another problem still remains which is the wider filter needed to capture the signal. A larger filter includes more noise which degrades system performance. As shown in Fig. 12 the performance of the DDBPSK method degrades drastically when the filter bandwidth increases. Inversely, the performance of ST-DFT method is not affected by different filter bandwidth values. This is due to the inherent characteristic of the ST-DFT analysis. ST-DFT can be interpreted as a bank of narrowband filters shown in Fig. 13 [13]. Each filter is a bandpass filter centered around frequency f_0. The impulse response of each filter is $w^*(-t)$ where $w(t)$ is the window function. Each bin of the ST-DFT is obtained via filtering signal with these bandpass filters (with corresponding center frequency) and then frequency shifting the result to baseband. Therefore, what influences the output of the analysis is not the bandwidth of the wide filter but the bandwidth of these narrowband filters constituting the ST-DFT analysis.

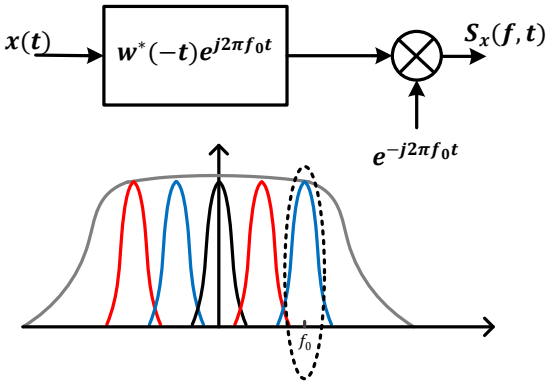

Fig. 13. Filter bank interpretation of Short Time Fourier Transform

B. Performance and complexity trade-off

Low power consumption is a crucial requirement for state-of-the-art wireless sensor networks. Basically, the idea of pushing the frequency offset tuning burden to the digital domain (for instance via using offset-robust demodulation methods) is to decrease power consumption in the receiver. Otherwise, a high quality crystal with thermal compensation must be used which increases power consumption considerably while it makes the communication node more costly. To achieve a better understanding of power consumption both BER performance and computational complexity must be taken into consideration. The BER curves of ST-DFT and DDPSK for FT=4 and FT=32 are demonstrated in Fig. 14. As can be seen depending on the required offset tolerance and target BER either of these methods might be preferable. Fig. 15 illustrates variations of required E_b/N_0 for *0.1%* BER in terms of filter bandwidth. It reveals that for a target BER of 0.1%, up to a certain point (*FT=8*) DDBPSK is superior to ST-DFT while afterwards ST-DFT outperforms DDBPSK. In fact after this point, the noise resulting from the wide filter dominates such that it outweighs the inherent limitations of BFSK over BPSK.

To compare the computational loads of these methods, an estimation of the number of the complex arithmetic operations needed for each symbol is listed in Table I where *M* is the number of samples per symbol or equivalently *FT* (as the sampling frequency is equal to the filter bandwidth). As expected, the ST-DFT method has a huge computational load compared to simple 2T-DDBPSK which is the cost paid for better performance in case of wider filters.

Fig. 14, Fig. 15 and Table I show the trade-off when the explained methods are employed. Based on the application at hand, the designer may consider one of these schemes. Digital complexity for Digital CMOS modern technology nodes (45nm or later technologies) is not a considerable loss, particularly, in a low data rate scenario which does not need high speed computation [15]. In such situations, achieving the same performance for different filter bandwidths leads to power saving which outweighs the additional complexity. On the other hand, for downlink communication between base station and a node (in case of a star topology), the transmitter power source is

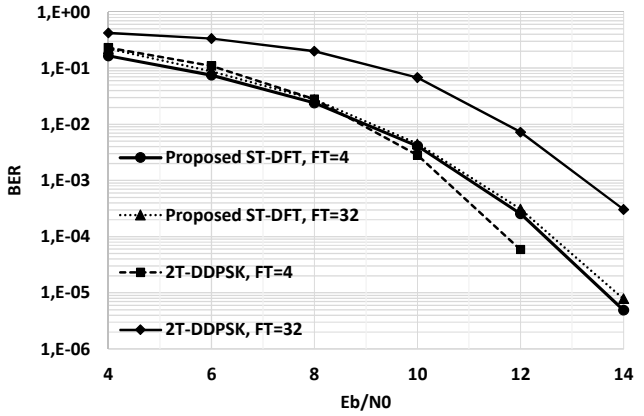

Fig. 14. Required E_b/N_0 for 0.1% BER for 2T-DDBPSK and ST-DFT

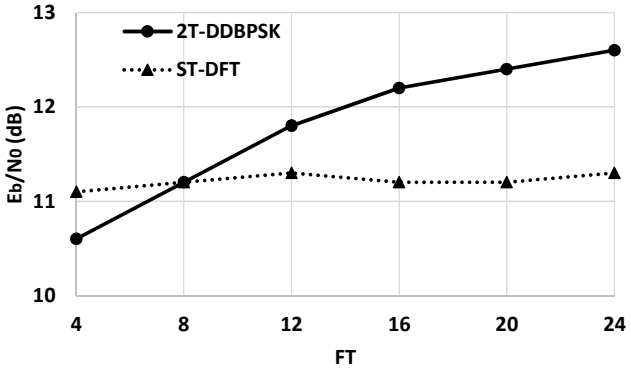

Fig. 15. Required E_b/N_0 for 0.1% BER for 2T-DDBPSK and ST-DFT

TABLE I ESTIMATED COMPUTATIONAL LOAD OF EACH DETECTION SCHEME BASED ON THE APPROXIMATE NUMBER OF COMPLEX ARITHMETIC OPERATIONS

	Detection (per symbol)	**Window Sync. (per packet)**
ST-DFT	$8Mlog(8M)$	$64M^2log(8M)$
2T-DDPSK	$2M$	-

considered to be sufficient to afford more BER performance loss. In this case DDBPSK keeps the complexity of the receiver low enough to have a low power receiver node.

VI. CONCLUSION

When the target is very low data rate communications in wireless sensor networks, frequency offset cancellation becomes challenging. It will require precise RF frequency generation which increases power consumption. Based on these facts using an offset tolerant method seems rational. In this paper a comparison between offset tolerant demodulators for DDBPSK and BFSK was made. For this purpose, an offset tolerant demodulator for BFSK was designed which is based on the ST-DFT. Its detection algorithm is simpler than a previous design based on ST-DFT while it achieves 1dB improvement in the BER performance. The power and complexity trade-off of these methods was discussed enabling the designer to have a better insight in selecting the best scheme based on configuration and further requirements of the target system. Considering the results, the DDBPSK method is promising in case of smaller frequency offset; whereas, in case of a very large frequency offset the ST-DFT method achieves better BER curves. The better performance of ST-DFT is provided at the expense of higher digital complexity which might be acceptable (compared to analog precise frequency generation or extra transmission power) in some applications and technology nodes.

REFERENCES

[1] I. F. Akyildiz, W. Su, Y. Sankarasubramaniam, and E. Cayirci,

"Wireless sensor networks: a survey," *Comput. Networks*, vol. 38, no. 4, pp. 393–422, 2002.

[2] D. Lachartre, F. Dehmas, C. Bernier, C. Fourtet, L. Ouvry, F. Lepin, E. Mercier, S. Hamard, L. Zirphile, S. Thuries, and F. Chaix, "7.5 A TCXO-less 100Hz-minimum-bandwidth transceiver for ultra-narrow-band sub-GHz IoT cellular networks," *2017 IEEE International Solid-State Circuits Conference (ISSCC)*. pp. 134–135, 2017.

[3] M. Morelli and U. Mengali, "Feedforward carrier frequency estimation with MSK-type signals," *IEEE Commun. Lett.*, vol. 2, no. 8, pp. 235–237, 1998.

[4] D. A. Gudovskiy, L. Chu, and S. Lee, "A Novel Nondata-Aided Synchronization Algorithm for MSK-Type-Modulated Signals," *IEEE Commun. Lett.*, vol. 19, no. 9, pp. 1552–1555, 2015.

[5] H. B. Çelebi and H. Arslan, "A joint blind carrier frequency and phase offset detector and modulation order identifier for MPSK signals," *2010 IEEE Radio Wirel. Symp. RWW 2010 - Pap. Dig.*, pp. 348–351, 2010.

[6] J. Sun and X. Li, "Carrier frequency offset synchronization algorithm for short burst communication system," *2016 IEEE 13th International Conference on Signal Processing (ICSP)*. pp. 1231–1235, 2016.

[7] R. Mehlan, Y. E. Chen, and H. Meyr, "A Fully Digital Feedforward MSK Demodulator with Joint Frequency Offset and Symbol Timing Estimation for Burst Mode Mobile Radio," *IEEE Trans. Veh. Technol.*, vol. 42, no. 4, pp. 434–443, 1993.

[8] E. Lopelli, J. D. Van der Tang, and A. H. M. van Roermund, "A FSK demodulator comparison for ultra-low power, low data-rate wireless links in ISM bands," *Proceedings of the 2005 European Conference on Circuit Theory and Design, 2005.*, vol. 2. p. II/259–II/262 vol. 2, 2005.

[9] M. K. Simon and D. Divsalar, "On the Implementation and Performance of Single and Double Differential Detection Schemes," *IEEE Trans. Commun.*, vol. 40, no. 2, pp. 278–291, 1992.

[10] M. R. Yuce and W. Liu, "A low-power multirate differential PSK receiver for space applications," *IEEE Trans. Veh. Technol.*, vol. 54, no. 6, pp. 2074–2084, 2005.

[11] S. Hara, A. Wannasarnmaytha, Y. Tsuchida, and N. Morinaga, "A novel FSK demodulation method using short-time DFT analysis for LEO satellite communication systems," *IEEE Trans. Veh. Technol.*, vol. 46, no. 3, pp. 625–633, 1997.

[12] E. Grayver and B. Daneshrad, "VLSI implementation of a 100-& multirate FSK receiver," *Solid-State Circuits, IEEE J.*, vol. 36, no. 11, pp. 1821–1828, 2001.

[13] F. Hlawatsch and G. F. Boudreaux-Bartels, "Linear and quadratic time-frequency signal representations," *IEEE Signal Processing Magazine*, vol. 9, no. 2. pp. 21–67, 1992.

[14] J. O. Smith, *Spectral Audio Signal Processing*. W3K, 2011.

[15] H. Kaul, M. A. Anders, S. K. Mathew, S. K. Hsu, A. Agarwal, R. K. Krishnamurthy, and S. Borkar, "A 300 mV 494GOPS/W reconfigurable dual-supply 4-way SIMD vector processing accelerator in 45 nm CMOS," *IEEE J. Solid-State Circuits*, vol. 45, no. 1, pp. 95–102, 2010.